Investigation of multiwall carbon nanotube-based nanofluid advantages in microchannel heat sinks

Reza Kamali[1], *Yaghoub Jalali*[2], *Alireza R. Binesh*[1]

[1]*School of Mechanical Engineering, Shiraz University, Shiraz 71348-51154, Iran*
[2]*Department of Mechanical Engineering, Hormozgan University, Bandarabbas 76548-37543, Hormozgan, Iran*
E-mail: rkamali@shirazu.ac.ir

Published in Micro & Nano Letters; Received on 19th October 2012; Revised on 19th April 2013; Accepted on 26th April 2013

In this Letter, the cooling performance of microchannel heat sinks, as well as a comparison of the heat the transfer efficiency of two nanofluids: Al_2O_3–water and multiwall carbon nanotube (MWCNT)–water and pure water, is investigated. At first, the same pumping power inlet boundary condition, which is a standard comparison of the performance of different fluids, is applied for a single rectangular duct, and the results are stored for the modelling of the heat sink. Following this stage, a heat sink made up of aluminium with water as working fluid is modelled. After validation of the results and optimisation of the grid, the efficiency of the three fluids is compared. It is seen that by using MWCNT–water nanofluid instead of water in a typical heat sink, the mean reduction in thermal resistance for MWCNT–water and Al_2O_3–water, in comparison with using water, respectively, are 18 and 1%. This shows the great advantages of using MWCNTs in heat sinks in comparison with Al_2O_3.

1. Introduction: Increasing heat generation in electrical devices has led to offering thousands of new scientific plans for cooling methods. One of the offered methods for electrical devices with high heat generation is using forced convection in microchannels as heat sinks. Studying microchannel heat sinks (MCHS) as heat exchangers was started by Tuckerman and Pease [1] in 1981, as they wrote an article about the usefulness of employing very small diameter channels for cooling electrical circuits. They stated that by decreasing the channels' diameter, the heat transfer coefficient would rise. Also, it was reported that the heat transfer coefficient of microchannels was 40 times higher than typical heat exchangers [1]. Since publication of that article, many investigations have been conducted on fabrication methods and augmentation in the performance of microchannels.

Excluding numerical studies accomplished based on porous media models [2–6], which have all been reviewed by Chen and Ding [7], newer studies are modelled by typical fluid flow equations (continuity, Navier-Stokes and energy equations) using finite volume methods. For instance, Toh *et al.* [8] have performed three-dimensional modelling of fluid flow and heat transfer inside heated microchannels. They have investigated the laminar steady form of momentum and energy equations using the finite volume method. They reported that incoming heat decreases friction losses and viscosity. This effect would cause higher temperatures especially at lower Reynolds numbers. Tiselj *et al.* [9] performed a numerical and experimental study over the effect of axial convection on heat transfer in triangular cross-section microchannels. They concluded that the wall temperature and the bulk temperature change nonlinearly along the channel.

As have many other scientists motivated by great developments in heat transfer after using nanofluids, Jang and Choi [10] surveyed the performance of an MCHS using nanofluids. Their study concluded that using diamond particles in the base fluid improves the thermal performance of an MCHS by about 10% at the same pumping power. In a similar study, Mohammed *et al.* [11] investigated the influence of particle volume fraction available in water–alumina nanofluid on the heat removal capabilities of rectangular channel shape MCHSs. They reported that by increasing the volume fraction of Al_2O_3, the heat transfer coefficient and shear stress increase and thermal resistance decreases.

In this study, an investigation was conducted into three types of fluids [multiwall carbon nanotube (MWCNT)–water nanofluid, alumina–water nanofluid and pure water]. Heat transfer performance through a straight rectangular microchannel for laminar flow in constant heat flux condition was performed first and then a typical heat sink was modelled to see the amount of enhancement caused by nanofluids usage.

2. Computational model

2.1. Geometry of the problem: Dimensions of a single microchannel used in this numerical modelling are shown in Fig. 1*a*. A three-dimensional microchannel with 1 cm length and a 280 × 430 μm rectangular cross-section is used as configuration of the problem. According to Fig. 1 and two symmetry axes, to reduce computations, for modelling a single microchannel, a solution is found only for a quarter of microchannels (only the blue cube). In order to model the whole MCHS, 26 microchannels were used, similar to the one shown in Fig. 1, and each two are 500 μm spaced. The overall dimensions of the MCHS is 10 090 μm × 1430 μm × 1 cm. Only the top wall of the MCHS is subjected to a non-zero heat flux (500 000 W/m^2), hence because of the symmetry shown in Fig. 1*b*, half of the MCHS is modelled (13 microchannels).

2.2. Governing equations: A single phase model is used for three-dimensional, steady-state and laminar forced flow of nanofluids in all cases of this study. Nanofluids were supposed to be, incompressible and excluding MWCNT–water, Newtonian. Hence, continuity, momentum and energy equations are as follows [12]:

Continuity equation

$$\nabla.\boldsymbol{V} = 0 \tag{1}$$

Momentum equation

$$\rho_{\mathrm{nf}}(\boldsymbol{V}.\nabla)\boldsymbol{V} = -\nabla P + \nabla.\left(\mu_{\mathrm{nf}}\nabla\boldsymbol{V}\right) \tag{2}$$

Energy equation

$$\rho_{\mathrm{nf}}Cp_{\mathrm{nf}}(\boldsymbol{V}.\nabla T) = \nabla.\left(k_{\mathrm{nf}}\nabla T\right) \tag{3}$$

In the above equations, Cp_{nf}, K_{nf}, $\boldsymbol{V}$, P and T are, respectively,

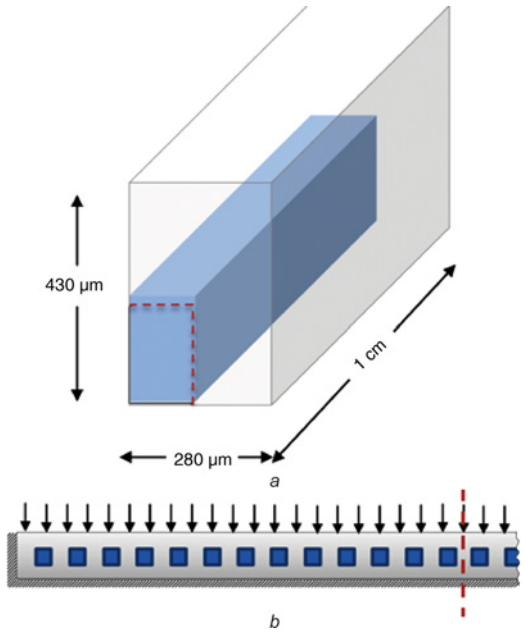

Figure 1 *Schematic of single microchannel used in MCHS (Fig. 1a), symmetry of MCHS and thermal boundary conditions (front and back walls are adiabatic) (Fig. 1b)*

density, viscosity, heat capacity, thermal conductivity, velocity vector, pressure and temperature (all related to working fluid).

2.3. Boundary conditions: Boundary conditions are described in this Section. To build up a more proper standard in the comparison of the performance of different fluids, the same pumping power inlet boundary condition was applied for a single rectangular duct, and the results were stored for the modelling of the heat sink.

First, we used our solver to find the flow field properties in a quarter of the rectangular microchannel for pure water. The Reynolds number considered in this process ranged from 100 to 1000. At the entrance of the microchannel uniform velocity was applied. It was calculated based on the desired Reynolds number and zero gauge pressure was exerted to the outlet of the microchannel, hence [11]

$$u_{\text{in}} = \frac{\text{Re}\mu}{\rho_{\text{nf}} D_{\text{h}}} \tag{4}$$

$$D_{\text{h}} = \frac{4A}{P} = \frac{2H_{\text{ch}}W_{\text{ch}}}{H_{\text{ch}} + W_{\text{ch}}} \tag{5}$$

in which, H_{ch} and W_{ch} are area, perimeter, height and width of the microchannel, respectively.

After that the solution was found, the mean value of the pressure at the inlet of the channel which has an unknown functionality of inlet velocity, was used to calculate pumping power using this formula

$$\text{Pumping power} = Q\Delta p \tag{6}$$

where Q is the volume flow rate calculated from $Q = u_{\text{in}} \times A$ and $\Delta p = p_{\text{in}} - p_{\text{out}}$ is the pressure drop in the channel ($p_{\text{out}} = 0$). Table 1 shows the calculated pumping power needed for water to flow through the microchannel, which was then used for the other two nanofluids.

After finding the values of pumping power, these values were used to define the new inlet boundary condition for channels. However, it is a complicated boundary type, because Δp in (6), is unknown at the beginning of the solution and is achieved from the end of the solution. Hence, we need a trial and error procedure to find the desired u_{in} that leads to a definite pumping power calculated from (6). Definite changeable inlet velocity was simply utilised as the boundary condition for this stage of our study. After some iterations (20–100 seems to be suitable for this problem), gaining an approximation of mean pressure at the inlet, the inlet velocity was recalculated based on pumping power and p_{in} by

$$u_{\text{in}}^{k+1} = u_{\text{in}}^{k} - \frac{u_{\text{in}}^{k} p_{\text{in}}^{k} - (\text{Pumping power}/A)}{p_{\text{in}}^{k} - u_{\text{in}}^{k}\left(\left(p_{\text{in}}^{k} - p_{\text{in}}^{k-1}\right)/\left(u_{\text{in}}^{k} - u_{\text{in}}^{k-1}\right)\right)} \tag{7}$$

Note that after some iteration, changes in u_{in}^{k+1} go down and it is not necessary to use (7). Using this algorithm, the equivalent inlet velocities for pumping powers from Table 1 were found and are listed in Table 2 for the two nanofluids.

Thermal boundary conditions were, uniform 300 K temperature at the inlet of each microchannel of the MCHS and constant 500 000 (W/m^2) top wall heat flux. Other outer surfaces of the MCHS were adiabatic. The following relations are used for solid fluid interfaces

$$\boldsymbol{V} = 0, \quad \theta = \theta_{\text{s}}, \quad -k_{\text{s}}\frac{\partial \theta_{\text{s}}}{\partial n} = -k\frac{\partial \theta}{\partial n} \tag{8}$$

2.4. Thermophysical and rheological properties of fluids: To date, no general analytical correlation is proposed for the thermal conductivity and viscosity of MWCNT–water nanofluid, therefore we should rely on experimental data. Experimental data submitted for 1 wt% MWCNT–water [13], besides corresponding formula gain by curve fitting techniques [12] are available references about the thermophysical and rheological properties of MWCNT–water nanofluid. To compare Al_2O_3–water, MWCNT–water and

Table 1 Pumping power used for inlet boundary condition

Re (pure water)	Pumping power, W
100	3.72060E-06
200	1.59593E-05
300	3.83051E-05
400	7.22221E-05
500	1.19017E-04
600	1.79862E-04
700	2.55841E-04
800	3.47906E-04
900	4.56952E-04
1000	5.83853E-04

Table 2 Inlet velocities used for modelling heat sinks and comparison of fluids

Pumping power, W	Pure water u_{in}, m/s	Al_2O_3–water u_{in}, m/s	MWCNT–water u_{in}, m/s
3.72060E-06	0.236177	0.233617	0.212300
1.59593E-05	0.472353	0.467316	0.427939
3.83051E-05	0.708530	0.701054	0.645450
7.22221E-05	0.944707	0.934814	0.864146
1.19017E-04	1.180880	1.168620	1.083605
1.79862E-04	1.417060	1.402367	1.303512
2.55841E-04	1.653240	1.636206	1.523702
3.47906E-04	1.889410	1.869992	1.744080
4.56952E-04	2.125590	2.103795	1.964466
5.83853E-04	2.361770	2.337570	2.185002

doi: 10.1049/mnl.2012.0803

Table 3 Thermophysical and rheological properties used in simulations

Properties	MWCNT–water	Al_2O_3–water	Base fluid
ρ, kg/m^3	1080	995	1022.4
Cp, J/kg·K	4181	4058.84	4150
k, W/m·K	0.617	0.633	$-287.6 + 3.022T - 0.010557T^2 + 1.2288 \times 10^{-5}T^3$
μ, Ns/m	0.000797	0.000815	$= \kappa\dot{\gamma}^{n-1}$, ($\kappa = 0.00135$, $n = 0.96$)

pure water heat transfer performance, we had to add same nanoparticle volume fractions to pure water. First of all, we found the corresponding volume fraction of MWCNT in water to 1wt% MWCNT–water nanofluid, which resulted in $\phi = 0.921\%$. Then, we discovered the properties of Al_2O_3–water, $\phi = 0.921\%$, by the following formulae [11]:

Density

$$\rho_{\text{nf}} = (1 - \varphi)\rho_{bf} + \varphi\,\rho_p \tag{9}$$

Heat capacity

$$Cp_{\text{nf}} = \left[(1 - \varphi)\left(\rho Cp_{bf}\right) + \varphi\left(\rho Cp_p\right)\right]/\rho_{\text{nf}} \tag{10}$$

Thermal conductivity

$$k_{\text{nf}} = \frac{k_p + 2k_{bf} + 2\left(k_p - k_{bf}\right)\varphi}{k_p + 2k_{bf} - \left(k_p - k_{bf}\right)\varphi}k_{bf} \tag{11}$$

Viscosity

$$\mu_{\text{nf}} = \mu_{bf}(1 + 2.5\varphi) \tag{12}$$

the results for various properties for the three fluids at 30°C are shown in Table 3.

3. Numerical method: A segregated solution algorithm with a finite volume-based technique is used in the numerical method. In this technique, integration of the governing equations of mass, momentum and energy on each cell within the computational domain is carried out to construct algebraic equations for unknown variables. Coupling of pressure and velocity was achieved by using the SIMPLE algorithm, which uses a predict-correct procedure for calculation of pressure on the grid arrangement. The second-order upwind scheme was used for discretisation of the equations as it is always stable for the pressure-correction equation.

4. Validation of the results: To find out whether we had obtained correct results from the numerical simulation or not, first of all we exerted the H2 boundary condition to a single microchannel. Results for the application of the H2 boundary condition in the rectangular duct are shown in Table 4. Looking at the errors tells

Table 4 Mean Nusselt number result of various grid densities for H2 boundary condition

Number of nodes	*Nu*	[a]Error, %
28 × 43 × 67	4.906	–
20 × 30 × 56	4.916	0.21
14 × 22 × 33	4.957	0.82
7 × 11 × 17	5.111	3.01

[a]Relative to the grid with more nodes

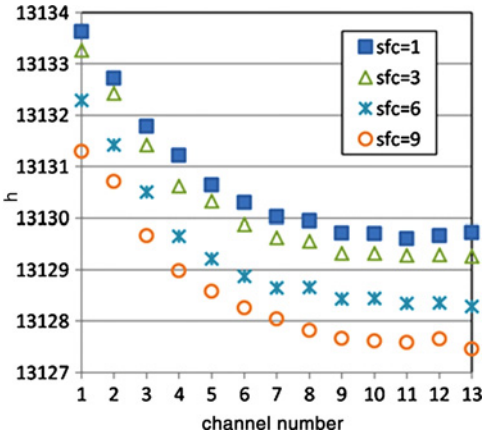

Figure 2 *Effect of sfc on mean heat transfer coefficient of each microchannel*

us that choosing the grid with 14 × 22 × 33 nodes is our optimum grid.

After studying grid independency for a single microchannel, all channels in the heat sink were meshed with the optimum grid introduced above. Hence, it was necessary just to investigate grid compactness in solid zones. To prevent new errors at the length of the MCHS's body, the number of nodes on the longitude of the heat sink are the same as microchannels fluid cells. However, in the cross-section of the heat sink, we had bigger cell faces to reduce computational cells, which means node-to-node spaces in the solid zone were more than in the fluid zone. 'Sfc' is the ratio of distances between nodes in the cross-section of the solid zone to that of the fluid zone. The effect of sfc on the solution accuracy for the heat transfer coefficient for each microchannel, h is plotted in Fig. 2. After examining the results, it seemed that the conduction equation in the solid zone does not need a dense grid structure. Hence, sfc = 6 can be a good ratio. Surprisingly, the relative error of sfc = 6 in proportion to sfc = 1 is about 0.01%. Taking 14 × 22 × 33 grid points in

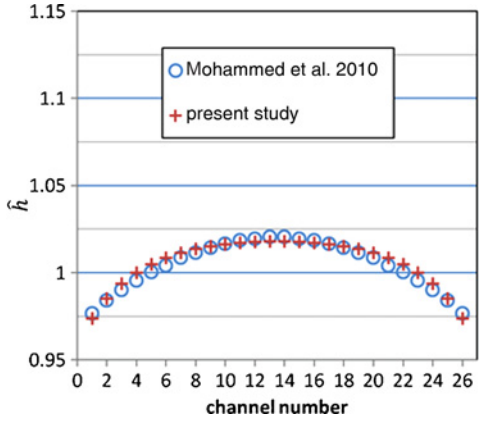

Figure 3 *Comparison of non-dimensional heat transfer coefficient gain by present study with that of reference [11]*

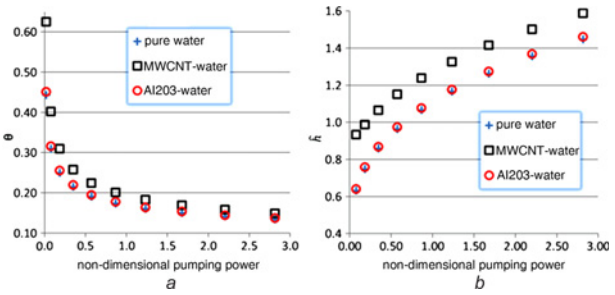

Figure 4 *Non-dimensional temperature (Fig. 4a), and non-dimensional heat transfer coefficient of Al_2O_3–water, MWCNT–water and pure water along microchannel*

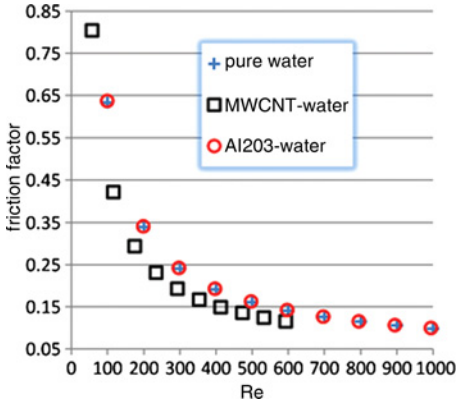

Figure 5 *Friction factor for Al_2O_3–water, MWCNT–water and pure water against Reynolds number*

each microchannel and sfc = 6 for the solid zone, there were about 629 013 computational cells in the MCHS. Here, it should be mentioned that this number of nodes required more computation time and we had to reduce the number of nodes in a manner that did not affect the accuracy much. Accordingly, all node-to-node distances were scaled 1.43 times bigger than earlier, which resulted in 220 271 total cells, surprisingly it only brought about 0.45% additional error. At the end of this section to validate our MCHS modelling results, we compared them with the same case from the work of Mohammed *et al.* [11]. As shown in Fig. 3, the present study has done well on prediction of $\hat{h}$.

5. Results: Knowing that our numerical model produces proper results, we examined the three fluids by changing the flowing fluid's properties and inlet velocities based on Tables 2 and 3, respectively. Distribution of the non-dimensional temperature of the first microchannel, calculated from (13), for the three investigated fluids against non-dimensional employed pumping power is shown in Fig. 4*a*. Non-dimensional pumping power is gained by dividing the values of pumping power in Table 2 by their mean value.

$$\theta = \frac{T_f - T_i}{T_{w,avg} - T_i} \tag{13}$$

According to Fig. 4*a*, non-dimensional temperature is higher for MWCNT–water. The reason is that the wall and fluid temperatures have less difference, leading to a higher heat transfer coefficient for this nanofluid than Al_2O_3–water and pure water, which is an advantage for CNT.

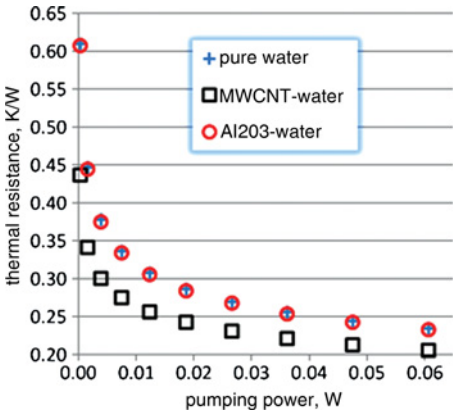

Figure 6 *R_{th} against pumping power for Al_2O_3–water, MWCNT–water and pure water*

The non-dimensional heat transfer coefficient for the three fluids is calculated from this equation [11]

$$\hat{h} = \frac{h}{h_{avg,water}} \tag{14}$$

where h is the heat transfer coefficient of the fluid and $h_{avg,water}$ is the average heat transfer coefficient of pure water. In Fig. 4*b*, the first microchannel of the heat sink is compared for the three fluids. According to Fig. 4*b*, heat transfer coefficient improvement for MWCNT–water, in comparison with the two other fluids, is great. Mean betterment of the heat transfer coefficient in the heat sink towards pure water, is 2% for Al_2O_3–water and 36% for MWCNT–water. This enhancement was our motivation to perform this study.

Friction factor is an important factor in the fluid's pressure drop, which is calculated by means of the Darcy equation [14]

$$f = \frac{2D_h \Delta p}{\rho_{nf}\, u_{in}^2\, L_{ch}} \tag{15}$$

In the above equation, D_h, Δp, ρ_{nf}, u_{in} and L_{ch} are the hydraulic diameter, pressure drop, density of the nanofluid, inlet velocity of the nanofluid and length of the microchannel, respectively. The effect of nanoparticles on the friction factor of pure water is presented in Fig. 5. It is obvious that another advantage of using MWCNT nanoparticles is the reduction of the friction factor.

One of the most useful parameters in the examination of the cooling performance of microchannels is the thermal resistance of the microchannel. It is calculated through the following formula [11]

$$R_{th} = \frac{T_{w,max} - T_{in}}{q_w}$$

However, plotting R_{th} against the Reynolds number does not help to prove that MWCNT can enhance the performance of MCHSs better than Al_2O_3 nanoparticles. To solve this, we used pumping power, which is the required power to drive the coolant in the microchannel, as the variable of the other axis. Fig. 6 shows R_{th} of the microchannel against pumping power. The main point in this Figure, which determines our study's outcome, is that MWCNT shows better results than alumina. By the same pumping power, MWCNT–water nanofluid has less thermal resistance and consequently higher cooling performance than the other two fluids. On the other hand, for the same thermal resistance MWCNT–water nanofluid needs less pumping power than the two other fluids (follow horizontal grid lines in Fig. 6). Mean thermal resistance

doi: 10.1049/mnl.2012.0803

reduction for using MWCNT–water nanofluid and Al_2O_3–water nanofluid proportional to pure water, are 18 and 1%. This great enhancement tells us that MWCNT is a better nanoparticle in increasing water's thermal efficiency than Al_2O_3.

6. Conclusion: In this Letter, the study of three fluids' (MWCNT–water, alumina–water and pure water) heat transfer performance through a straight rectangular microchannel for laminar flow in constant heat flux condition was performed first and then a typical heat sink was modelled to see the amount of enhancement caused by nanofluids usage. For simulation of nanofluids' flow, incompressible Navier-Stokes equations uncoupled with an energy equation were solved numerically using the finite volume method. This study was performed to prove that MWCNT is a better nanoparticle than Al_2O_3 in the enhancement of the cooling performance of pure water. The results show that using MWCNT-based nanofluid has several advantages in the cooling of microchannels and MCHSs over alumina-based nanofluid or pure water; lower non-dimensional temperature and friction factor in addition to higher heat transfer coefficient and thermal resistance for working fluid are some of these advantages. In addition, it is seen that for the same pumping power, MWCNT–water nanofluid has less thermal resistance, maximum wall temperature and consequently higher cooling performance than alumina–water nanofluid. However, it supports the idea that 1vol. % of alumina enhances water cooling performance.

7 References

[1] Tuckerman D.B., Pease R.F.: 'High performance heat sinking for VLSI', *IEEE Electron Device Lett.*, 1981, **2**, (5), pp. 126–129

[2] Phillips R.J.: 'Microchannel heat sinks', in Bar-Cohen A. (Ed.): 'Advances in thermal modeling of electronic components and systems' (ASME Press, New York, 1990), Chap. 3, pp. 109–122

[3] Vafaei K., Tien C.L.: 'Boundary and inertia effects on flow and heat transfer in porous media', *Int. J. Heat Mass Transf.*, 1981, **24**, pp. 195–203

[4] Poulikakos P., Renken K.: 'Forced convection in a channel filled with porous medium, including the effects of flow inertia, variable porosity, and Brinkman friction', *ASME J. Heat Transf.*, 1987, **109**, pp. 880–888

[5] Chen C.-H.: 'Analysis on non-Darcy mixed convection from impermeable horizontal surfaces in porous media-the entire regime', *Int. J. Heat Mass Transf.*, 1997, **40**, pp. 2993–2997

[6] Chen C.-H.: 'Forced convection heat transfer in microchannel heat sinks', *Int. J. Heat Mass Transf.*, 2007, **50**, pp. 2182–2189

[7] Chen C.-H., Ding C.-Y.: 'Study on the thermal behavior and cooling performance of a nanofluid-cooled microchannel heat sink', *Int. J. Thermal Sci.*, 2011, **50**, (3), pp. 378–384

[8] Toh K.C., Chen X.Y., Chai J.C.: 'Numerical computation of fluid flow and heat transfer in microchannels', *Int. J. Heat Mass Transf.*, 2002, **45**, pp. 5133–5141

[9] Tiselj I., Hetsroni G., Mavko B., *ET AL.*: 'Effect of axial conduction on the heat transfer in microchannels', *Int. J. Heat Mass Transf.*, 2004, **47**, pp. 2551–2565

[10] Jang S.P., Choi S.U.S.: 'Cooling performance of a microchannel heat sink with nanofluids', *Appl. Therm. Eng.*, 2006, **26**, pp. 2457–2463

[11] Mohammed H.A., Gunnasegaran P., Shuaib N.H.: 'Heat transfer in rectangular microchannels heat sink using nanofluids', *Int. Commun. Heat Mass Transf.*, 2010, **37**, (10), pp. 1496–1503

[12] Kamali R., Binesh A.R.: 'Numerical investigation of heat transfer enhancement using carbon nanotube-based non-Newtonian nanofluids', *Int. Commun. Heat Mass Transf.*, 2010, **37**, pp. 1153–1157.

[13] Garg P., Alvarado J.L., Marsh C.H., *ET AL.*: 'An experimental study on the effect of ultrasonication on viscosity and heat transfer performance of multi-wall carbon nanotube-based aqueous nanofluids', *Int. J. Heat Mass Transf.*, 2009, **52**, pp. 5090–5101

[14] Moody L.F.: 'Friction factors for pipe flow', *J. Heat Transf.*, 1944, **66**, pp. 671–684